

Magnetic fullerenes inside single-wall carbon nanotubes

F. Simon,^{1,3} H. Kuzmany,¹ B. Náfrádi,² T. Fehér,^{2,3} L. Forró,² F. Fülöp,³

A. Jánosy,³ L. Korecz,⁴ A. Rockenbauer,⁴ F. Hauke,⁵ and A. Hirsch⁵

¹*Institut für Materialphysik, Universität Wien, Strudlhofgasse 4, A-1090 Wien, Austria*

²*Institute of Physics of Complex Matter, FBS Swiss Federal Institute of Technology (EPFL), CH-1015 Lausanne, Switzerland*

³*Budapest University of Technology and Economics,*

Institute of Physics and Solids in Magnetic Fields Research Group of the Hungarian Academy of Sciences, H-1521, Budapest P.O.Box 91, Hungary

⁴*Chemical Research Center, Institute of Chemistry, P.O.Box 17, H-1525 Budapest, Hungary and*

⁵*Institut für Organische Chemie der Friedrich Alexander Universität Erlangen-Nürnberg, Henkestrasse 42, D - 91054 Erlangen*

C₅₉N magnetic fullerenes were formed inside single-wall carbon nanotubes by vacuum annealing functionalized C₅₉N molecules encapsulated inside the tubes. A hindered, anisotropic rotation of C₅₉N was deduced from the temperature dependence of the electron spin resonance spectra near room temperature. Shortening of spin-lattice relaxation time, T_1 , of C₅₉N indicates a reversible charge transfer toward the host nanotubes above ~ 350 K. Bound C₅₉N-C₆₀ heterodimers are formed at lower temperatures when C₆₀ is co-encapsulated with the functionalized C₅₉N. In the 10-300 K range, T_1 of the heterodimer shows a relaxation dominated by the conduction electrons on the nanotubes.

Single-wall carbon nanotubes (SWCNTs) [1, 2] exhibit a variety of unusual physical phenomena related to their one-dimensional and strongly correlated electronic properties. These include excitonic effects [3, 4], superconductivity [5], the Tomonaga-Luttinger liquid state [6], and the Peierls transition [7]. Magnetic resonance is a powerful method to study strong correlations in low dimensional systems. However, for SWCNTs both nuclear magnetic resonance (NMR) and electron spin resonance (ESR) are severely limited by NMR active ¹³C nuclei and ESR active electron spins in residual magnetic catalytic particles and other carbon phases. Synthesis of ¹³C isotope engineered SWCNTs solved the problem for NMR [8, 9]. To enable ESR spectroscopy of SWCNTs, a local probe, specifically attached to SWCNTs, is required. The N@C₆₀ [10] and C₅₉N [11] magnetic fullerenes are ideal candidates for such studies. In fullerene doped SWCNTs, fullerenes occupy preferentially the interior of the tubes and form "peapods" (C₆₀@SWCNT) [12]. Fullerenes adhering to the outside can be removed [13] in contrast to e.g. filling with iron [14]. ESR on encapsulated magnetic fullerenes could yield information on the electronic state of the tubes and it could also enable to study the fullerene rotational dynamics in a confined environment. In addition, magnetic fullerene peapods could exploit the combination of the SWCNT strength and the magnetic moment of molecules in magnetic scanning probe tips and they could enable a bottom-up design for magnetic storage devices or for building elements of quantum computers [15].

Typical spin concentrations in (N@C₆₀:C₆₀)@SWCNT are low, ~ 1 spin/tube, and the N spins are insensitive to SWCNT properties [16]. The C₅₉N monomer radical is a better local probe candidate as the unpaired electron is on the cage. C₅₉N can be chemically prepared but it forms spinless dimers (C₅₉N)₂ or monomer adducts [11].

The magnetic C₅₉N monomer radical can be stabilized as C₅₉N:C₆₀, a dilute solid solution of C₅₉N in C₆₀ [17].

Here, we report on the first ESR study of SWCNT properties and peapod rotational dynamics using a paramagnetic local probe: C₅₉N monomer radicals encapsulated inside SWCNTs. SWCNTs were first filled with chemically inert C₅₉N derivatives. A heat treatment in vacuum removes the side-group and the monomer radical is left behind. The rotation of encapsulated C₅₉N is hindered and anisotropic in contrast to the isotropic rotation in C₅₉N:C₆₀. In samples with co-encapsulated C₆₀ and C₅₉N, bound C₅₉N-C₆₀ heterodimers are formed during the heat treatment. The electron spin-relaxation time of the heterodimer is dominated by the conduction electrons of the SWCNTs and follows the Korringa law.

SWCNTs were filled with air stable C₅₉N derivatives (4-Hydroxy-3,5-dimethyl-phenyl-hydroza fullerene, C₅₉N-der in the following) and C₅₉N-der:C₆₀ in concentrations of 1:10. The mean value of the SWCNT diameter distribution, as determined from Raman studies [18], $d = 1.40$ nm is optimal for fullerene encapsulation. A mixture of dissolved fullerenes and SWCNTs were sonicated in toluene and filtered, which results in a high degree of encapsulation as shown by transmission electron microscopy and Raman spectroscopy in Ref. [19]. The peapods were mixed with ESR silent SnO₂ to separate the conducting SWCNT pieces and were annealed in dynamic vacuum at 600 °C for 15 minutes to remove the side-group. The air-sensitive materials were sealed under He in quartz tubes. ESR was studied on a Bruker Elexsys spectrometer at 9 GHz in the 10-600 K temperature range with spin-sensitivity calibrated by CuSO₄·5(H₂O).

Fig. 1 shows the room temperature ESR spectra of C₅₉N@SWCNT (sample A) and C₅₉N:C₆₀@SWCNT (sample B) and for comparison the spectrum of crys-

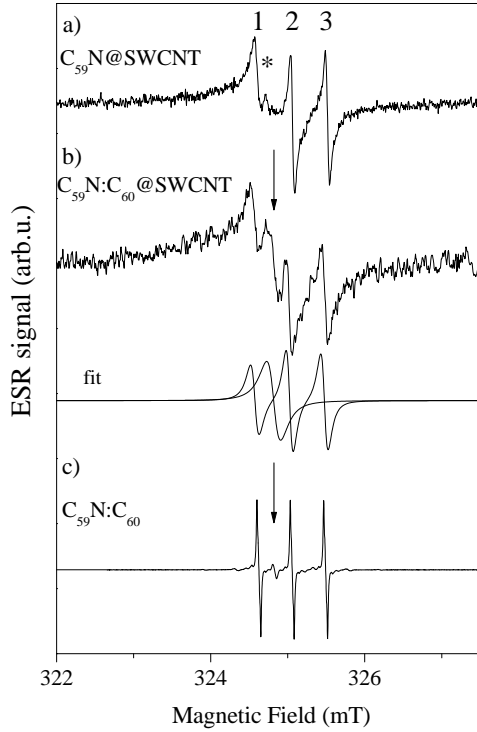


FIG. 1: ESR spectra of a) $C_{59}N@SWCNT$, b) $C_{59}N:C_{60}@SWCNT$, and c) crystalline $C_{59}N:C_{60}$ at 300 K. 1, 2, and 3 denote the ^{14}N hyperfine triplet lines with nuclear state of $I = 1, 0$, and -1 , respectively. Asterisk in a) shows a weak impurity signal. Arrows in b) and c) indicate the $C_{59}N-C_{60}$ heterodimer. Fit in b) shows the deconvolution of the ESR signal into the ^{14}N triplet of monomer $C_{59}N$ and the $C_{59}N-C_{60}$ heterodimer components.

talline $C_{59}N:C_{60}$ (sample C) from Ref. [17]. This latter spectrum was previously assigned to the superposition of rotating $C_{59}N$ monomers and bound $C_{59}N-C_{60}$ heterodimers [20]. The large spin density at the ^{14}N nucleus of the rotating $C_{59}N$ molecule results in an ESR triplet signal and the $C_{59}N-C_{60}$ heterodimer has a singlet signal (arrow in Fig. 1c) as the spin density resides on the C_{60} molecule. ^{14}N triplet structures are observed in the peapod samples (A and B) with identical hyperfine coupling as in the crystalline sample (C) and are thus identified as the ESR signals of rotating $C_{59}N$ monomer radicals encapsulated inside SWCNTs. The additional component (arrow in Fig. 1b) observed for sample B, which contains co-encapsulated C_{60} , is identified as $C_{59}N-C_{60}$ heterodimers encapsulated inside SWCNTs since this signal has the same g -factor as in the crystalline material. This singlet line is absent in sample A which does not contain C_{60} . For both peapod samples a broader line with HWHM of $\Delta H \sim 0.6$ mT is also observed. The broader component appears also on heat treatment of reference samples without encapsulated $C_{59}N$ -der and is identified as a side-product. Annealing at 600 °C is optimal: lower temperatures result in smaller $C_{59}N$ signals and higher

temperatures increase the broad impurity signal without increasing the $C_{59}N$ intensity.

Deconvolution of the ESR signal (Fig. 1b) and the intensity calibration against the $CuSO_4 \cdot 5(H_2O)$ spin standard allows to measure the amount of $C_{59}N$ related ($C_{59}N$ monomer and $C_{59}N-C_{60}$ heterodimer) spins in the sample. The amount of encapsulated fullerenes is known [8], thus the ratio, r , of observed $C_{59}N$ related spins and encapsulated $C_{59}N$ -der can be determined. We obtained $r = 2.5(6) \%$ and $r = 12(3) \%$ for the A and B samples, respectively. The observed ESR signal of $C_{59}N$ can be reduced due to various reasons: i) dimerization of $C_{59}N$ first neighbors into ESR silent $(C_{59}N)_2$, ii) incomplete transformation of $C_{59}N$ -der into $C_{59}N$, iii) dipolar fields of near neighbor $C_{59}N$ pairs: only those $C_{59}N$ related spins are observed which have no neighbors with dipole fields larger than the ESR line-width, ~ 0.07 mT. The likely origin of the smaller r value for sample A is dimerization. For sample B, however, a statistical calculation of the dipolar fields gives $r = 9 \%$ in agreement with the experimental value. For the calculation, the fullerene lattice constant inside the tubes [21], the three dimensional arrangement of the SWCNTs into bundles [22], the random orientation of the bundles, and the concentration of $C_{59}N$ was taken into account. As a result, the data for sample B supports that most $C_{59}N$ -der is transformed to $C_{59}N$ monomer radicals.

The temperature dependence of the line-widths of the ^{14}N triplet is identical for the two peapod samples, A and B, and is shown together with the data on $C_{59}N:C_{60}$ in Fig. 2 using the labeling given in Fig. 1a. The line-widths are ~ 0.04 mT larger for the peapod than for the crystalline material. This excess line-width is similar to that of $(N@C_{60}:C_{60})@SWCNT$ and is related to the stray magnetic field of magnetic catalytic particles in the nanotube sample [16]. The three $C_{59}N$ triplet lines are broadened unequally at lower temperatures for both the peapod and crystalline materials. The details of the low temperature broadening are different for the two kinds of materials: for encapsulated $C_{59}N$, the inequality persists to higher temperatures and the three lines broaden differently, whereas for the crystalline $C_{59}N:C_{60}$ line 1 broadens significantly and lines 2 and 3 broaden equally but less.

The unequal broadening of ^{14}N triplet lines with decreasing temperature is well known for NO spin labels and is explained by an incomplete motional narrowing of the anisotropic hyperfine and g -factor anisotropy [23]. For crystalline $C_{59}N:C_{60}$, molecular rotation becomes rapid enough immediately above the 261 K structural phase transition to result in motionally narrowed lines [17]. In contrast, the line-width data of encapsulated $C_{59}N$ indicates a hindered rotation. The line-width in the hindered molecular rotation regime is:

$$\Delta H = A + BM_I + CM_I^2 \quad (1)$$

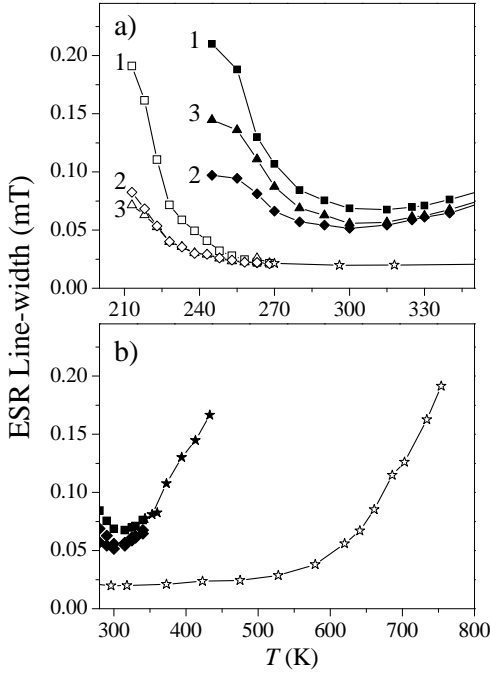


FIG. 2: Line-widths of the ^{14}N triplet components in crystalline $\text{C}_{59}\text{N}:\text{C}_{60}$ (open symbols) and $(\text{C}_{59}\text{N}, \text{C}_{59}\text{N}:\text{C}_{60})@\text{SWCNT}$ (full symbols) samples below 350 K (a) and above 290 K (b). Stars show the data for the temperature range where the line-widths of the three components are equal. Solid lines are guides to the eye.

where M_I is the nuclear state of the ^{14}N hyperfine lines and the parameters A , B , and C depend on the hyperfine and g -tensor components, on the R_x , R_y , and R_z molecular rotational rates around each axis, and on the ESR frequency [23]. For crystalline $\text{C}_{59}\text{N}:\text{C}_{60}$ at 9 GHz the isotropic rotation of the molecule (i.e. $R_x = R_y = R_z$) combined with the hyperfine and g -tensors results in $B \approx C$ and thus in an equal broadening for lines 2 ($M_I = 0$) and 3 ($M_I = -1$) [17, 20]. The inequality of the line-widths for encapsulated C_{59}N indicates an anisotropic rotation, i.e. $R_x \neq R_y \neq R_z$ as the hyperfine and g -tensor components are expected to be identical for the peapod and crystalline materials. The anisotropic rotation is suggested to originate from the anisotropic environment inside the nanotubes.

Above 300 K the triplet line-widths rapidly grow with temperature (Fig. 2b) and the signal intensity decreases faster than the Curie-law but no new lines appear. The broadening and the loss of signal intensity is fully reversible with temperature cycling. The broadening is reminiscent of that observed above ~ 600 K in the crystalline material, which was interpreted as a spin-lattice life-time shortening due to delocalization of the electron from C_{59}N over the C_{60} matrix [20]. Based on the analogous behavior, we suggest that reversible charge transfer from C_{59}N toward the nanotubes takes place above \sim

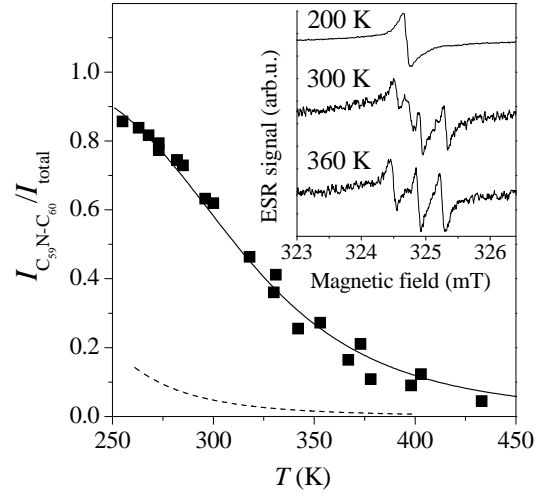


FIG. 3: Concentration of $\text{C}_{59}\text{N}-\text{C}_{60}$ bound heterodimers in $\text{C}_{59}\text{N}:\text{C}_{60}@\text{SWCNT}$. Solid curve is a fit with parameters explained in the text. Dashed curve shows the same quantity for crystalline $\text{C}_{59}\text{N}:\text{C}_{60}$ above the 261 K phase transition. Note the much higher heterodimer concentration for the peapod material. Inset shows the temperature evolution of the spectra.

350 K. The significantly lower temperature of the charge transfer indicates a larger overlap of the extra electron of C_{59}N to the SWCNTs compared to its overlap with the C_{60} conduction band in the crystalline material. In $\text{C}_{59}\text{N}:\text{C}_{60}$ the broadening is accompanied by the emergence of the ESR signal of the delocalized electrons. The intrinsic ESR signal of SWCNTs is not observable [24, 25], which explains the absence of a signal corresponding to charge transferred electrons on the tubes.

The coexistence of bound $\text{C}_{59}\text{N}-\text{C}_{60}$ heterodimers and rotating C_{59}N molecules was understood for $\text{C}_{59}\text{N}:\text{C}_{60}$ as a thermal equilibrium between the ground state heterodimer and the rotating monomers [20]. The inset in Fig. 3 shows a similar behavior for $\text{C}_{59}\text{N}:\text{C}_{60}@\text{SWCNT}$: the heterodimer dominates the low temperature spectrum and vanishes at higher temperatures, however the relative intensity of the heterodimer is much larger in this material. The heterodimer signal intensity normalized by the total (heterodimer+triplet) intensity gives the heterodimer concentration and is shown in Fig. 3. Similarly to crystalline $\text{C}_{59}\text{N}:\text{C}_{60}$, the heterodimer concentration can be fitted with:

$$\frac{I_{\text{C}_{59}\text{N}-\text{C}_{60}}}{I_{\text{total}}} = \frac{1}{(1 + e^{(-E_a/T + \Delta S)})} \quad (2)$$

where E_a is the binding energy of the heterodimer and ΔS is the entropy difference between the rotating monomer and the static heterodimer states. A fit with Eq. 2 for the peapod material is shown in Fig. 3 as a solid curve and gives $E_a(\text{peapod}) = 2800(200)$ K and

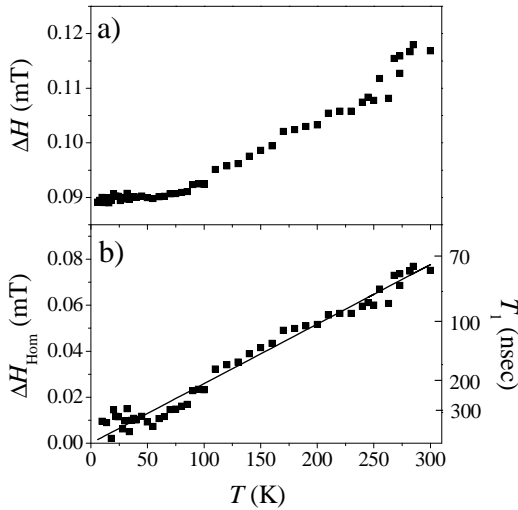


FIG. 4: a) Temperature dependence of the ESR line-width for the heterodimer signal. b) The homogeneous contribution to the line-width with a linear fit (solid line). The corresponding T_1 values are shown on the right axis.

$\Delta S(\text{peapod}) = 9(1)$. This compares to the results for the crystalline material with $E_a(\text{cryst}) = 2400(600)$ K and $\Delta S(\text{cryst}) = 11(2)$ [20]. The higher heterodimer concentrations for the peapod material is caused by the larger E_a and smaller ΔS values. The latter is explained by the limited rotational freedom of encapsulated C_{59}N .

Similar to NMR spectroscopy, the ESR spin-lattice relaxation time, T_1 , of the localized heterodimer spins yields information on the electronic structure of the host SWCNT material [26]. T_1 can be measured by time-resolved ESR measurements or in continuous wave ESR spectroscopy from the line-width, ΔH , by separating the homogeneous, relaxation related line-width from the inhomogeneous one. In Fig. 4a, we show ΔH for the heterodimer signal as determined from fits with derivative Lorentzian lines. Clearly, ΔH has a temperature dependent component in addition to a $\Delta H_0 = 0.089(2)$ mT residual line-width, which is obtained by averaging the line-widths below 50 K. The line-shape of the heterodimer signal does not change with temperature, which indicates a uniform, homogeneous broadening in addition to the inhomogeneous residual width.

To obtain the homogeneous line-width, ΔH_{Hom} , we subtracted ΔH_0 from the line-width data: $\Delta H_{\text{Hom}} = \sqrt{\Delta H^2 - \Delta H_0^2}$. Fig. 4b shows ΔH_{Hom} and $1/T_1 = \gamma_e \Delta H_{\text{Hom}}$, where $\gamma_e/2\pi = 28.0$ GHz/T is the electron gyromagnetic ratio. $1/T_1$ as a function of T is linear, with $(T_1 T)^{-1} = 4.2(2) \cdot 10^4 (\text{sK})^{-1}$ (fit shown in Fig. 4b), which suggests that Korringa relaxation, i.e. the interaction with conduction electrons [26] gives the relaxation of the heterodimer. An effective coupling constant (averaged for tube chiralities), A , of localized spins and conduction electrons is 11 meV as determined from the

Korringa relation [26]:

$$\frac{1}{T_1 T} = \left(\frac{4\pi k_B}{\hbar} \right) A^2 \bar{n}(E_F)^2 \quad (3)$$

where $\bar{n}(E_F) = 0.014$ states/eV/atom is the DOS at the Fermi level for a $d \approx 1.4$ nm metallic tube in the tight-binding approximation [22]. The above discussed uniformity of the homogeneous broadening suggests that the heterodimer spins do not sense separate metallic and semiconducting tubes as it would be expected based on the geometry of tubes alone [22]. This can be explained by charge transfer in the SWCNTs bundles, which shifts the Fermi level and renders all tubes metallic.

In summary, we observed C_{59}N monomer radicals encapsulated in SWCNTs. The nanotube cage hinders and makes the molecular rotation anisotropic. We find a low activation energy for charge transfer to the tubes. At low temperatures, bound $\text{C}_{59}\text{N}-\text{C}_{60}$ heterodimers are observed when mixtures of the two fullerenes are encapsulated. Electron spin-relaxation of the heterodimer shows an overall metallic behavior of the tubes. The material is a step toward the realization of confined linear spin-chains, which might find application in e.g. quantum information processing.

FS acknowledges the Zoltán Magyary programme for support. Work supported by the Austrian Science Funds (FWF) project Nr. 17345, by the Deutsche Forschungsgemeinschaft (DFG), by the EU projects MERG-CT-2005-022103 and BIN2-2001-00580 and by the Hungarian State Grants (OTKA) No. TS049881, F61733, PF63954, and NK60984.

* Corresponding author: ferenc.simon@univie.ac.at

-
- [1] S. Iijima and T. Ichihashi, *Nature* **363**, 603 (1993).
 - [2] D. S. Bethune *et al.*, *Nature* **363**, 605 (1993).
 - [3] C. D. Spataru *et al.*, *Phys. Rev. Lett.* **92**, 077402 (2004).
 - [4] F. Wang, G. Dukovic, L. E. Brus, and T. F. Heinz, *Science* **308**, 838 (2005).
 - [5] Z. K. Tang *et al.*, *Science* **292**, 2462 (2001).
 - [6] H. Ishii *et al.*, *Nature* **426**, 540 (2003).
 - [7] K. P. Bohnen *et al.*, *Phys. Rev. Lett.* **93**, 245501 (2004).
 - [8] F. Simon *et al.*, *Phys. Rev. Lett.* **95**, 017401 (2005).
 - [9] P. M. Singer *et al.*, *Phys. Rev. Lett.* **95**, 236403 (2005).
 - [10] T. Almeida Murphy *et al.*, *Phys. Rev. Lett.* **77**, 1075 (1996).
 - [11] J. C. Hummelen, C. Bellavia-Lund, and F. Wudl, *Heterofullerenes* (Springer, Berlin, Heidelberg, 1999), vol. 199, p. 93.
 - [12] B. W. Smith, M. Monthieux, and D. E. Luzzi, *Nature* **396**, 323 (1998).
 - [13] H. Kataura *et al.*, *Synthetic Met.* **121**, 1195 (2001).
 - [14] B. C. Satishkumar, A. Taubert, and D. E. Luzzi, *J. Nanosci. and Nanotechn.* **3**, 159 (2003).
 - [15] W. Harneit *et al.*, *Phys. St. Solidi B* **233**, 453 (2002).
 - [16] F. Simon *et al.*, *Chem. Phys. Lett.* **383**, 362 (2004).

- [17] F. Fülöp *et al.*, Chem. Phys. Lett. **334**, 223 (2001).
- [18] H. Kuzmany *et al.*, Eur. Phys. J. B **22**, 307 (2001).
- [19] F. Simon *et al.*, Carbon **44**, 1958 (2006).
- [20] A. Rockenbauer *et al.*, Phys. Rev. Lett. **94**, 066603 (2005).
- [21] K. Hirahara *et al.*, Phys. Rev. B **64**, 115420 (2001).
- [22] M. S. Dresselhaus, G. Dresselhaus, and P. Avouris, *Carbon Nanotubes: Synthesis, Structure, Properties, and Applications* (Springer, Berlin, Heidelberg, New York, 2001).
- [23] J. H. Freed, *Spin Labeling: Theory and Application* ed. L. J. Berliner, (Academic Press, New York, 1976), pp. 53–132.
- [24] A. S. Claye, N. M. Nemes, A. Jánossy, and J. E. Fischer, Phys. Rev. B **62**, 4845 (2000).
- [25] J.-P. Salvetat *et al.*, Phys. Rev. B **72**, 075440 (2005).
- [26] C. P. Slichter, *Principles of Magnetic Resonance* (Springer-Verlag, New York, 1989), 3rd ed.